Materials Research Express

INCLUSIVE PUBLISHING TRUSTED SCIENCE
PURPOSE-LED PUBLISHING™

PAPER • **OPEN ACCESS**

Comprehensive investigation of linear and nonlinear optical properties and tunable band gaps in CS/PVP-GnP nanocomposites

To cite this article: Ömer Bahadır Mergen and Ertan Arda 2026 *Mater. Res. Express* **13** 025002

View the article online for updates and enhancements.

You may also like

- Linear and nonlinear optical properties of PVC/PMMA polymer blends reinforced with TiO_2/GNP hybrid fillers for optoelectronics applications
A A Al-Muntaser, Eman Alzahrani, Abdullah F Al Naim et al.
- New Fabricated UHMWPEO-PVA Hybrid Nanocomposites Reinforced by GO Nanosheets: Structure and DC Electrical Behaviour
Nisreen R. Aldulaimi and Ehssan Al-Bermany
- Enhancing the optical absorption, conductivity, and nonlinear parameters of PVOH films by Bi-doping
H Elhosiny Ali, I S Yahia, H Algarni et al.

kiutra

Millikelvin characterization for superconducting devices

L-TYPE RAPID

- **< 4 hrs** sample loading and cooldown to base
- **50 mK** base temperature
- **30 min** warm up and sample exchange

Find out more →



This content was downloaded from IP address 194.27.52.199 on 26/10/2026 at 08:44

Materials Research Express

Check for updates

OPEN ACCESS

RECEIVED
14 October 2025

REVISED
1 January 2026

ACCEPTED FOR PUBLICATION
19 January 2026

PUBLISHED
30 January 2026

Original content from this work may be used under the terms of the Creative Commons Attribution 4.0 licence.

Any further distribution of this work must maintain attribution to the author(s) and the title of the work, journal citation and DOI.

PAPER

Comprehensive investigation of linear and nonlinear optical properties and tunable band gaps in CS/PVP-GnP nanocomposites

Ömer Bahadır Mergen[1,*] **and Ertan Arda**[2]

[1] Department of Medical Imaging Techniques, Dokuz Eylul University, Izmir, Türkiye
[2] Department of Physics, Faculty of Science, Trakya University, Edirne, Türkiye
[*] Author to whom any correspondence should be addressed.

E-mail: bahadir.mergen@deu.edu.tr

Keywords: CS/PVP-GnP nanocomposites, graphene nanoplatelets, optical dispersion models, wemple–DiDomenico analysis, nonlinear optical properties

Supplementary material for this article is available online

Abstract

The growing demand for low-cost and environmentally friendly polymer nanocomposites has intensified research efforts toward advanced functional materials. In this work, chitosan/polyvinylpyrrolidone (CS/PVP) nanocomposites reinforced with graphene nanoplatelets (GnP) were fabricated using a solution-based method and systematically characterized to evaluate their electrical and optical performance. The study focuses on electrical conductivity, optical band gap energy (E_g), Urbach energy (E_u), reflectance (R), refractive index (n), optical conductivity, and optical dielectric properties. To gain deeper insight into the dispersive and electronic behavior of the nanocomposites, the Wemple–DiDomenico (WD) model, the Spitzer–Fan model, and the Drude free-electron model were employed. In addition, the nonlinear optical (NLO) parameters, including optical susceptibility and nonlinear refractive indices, were analyzed. The results reveal significant enhancements in both linear and nonlinear optical properties with increasing GnP content, highlighting the strong structure–property relationships within the nanocomposite system. These findings demonstrate that CS/PVP-GnP nanocomposites are promising candidates for advanced applications in optoelectronics, energy storage, and photonic technologies.

1. Introduction

The convergence of materials science and nanotechnology has fostered the development of novel polymer composite materials with tunable properties, enabling their application across various industrial fields. In particular, a detailed examination of the optical properties of polymer composites plays a crucial role in identifying and optimizing their potential uses, advancing next-generation technologies, and enhancing existing systems. These polymer nanocomposites have attracted considerable attention for a wide range of technological applications, including optoelectronic devices (such as solar cells and LEDs) and energy storage systems [1–3]. In addition, numerous studies have explored their potential use in optical coatings [4], biomedical technologies (including biosensors and drug delivery systems) [5, 6], as well as photonic and laser-related applications [7], mainly through comprehensive investigations of their optical and electronic properties.

In recent years, there has been a growing interest in biodegradable and environmentally friendly polymer nanocomposites due to their potential to improve sustainability while tailoring material properties for advanced applications [8–11]. In this context, chitosan (CS) stands out as a biocompatible and non-toxic polysaccharide that is abundant in nature [12–15]. Chitosan is particularly recognized for its film-forming and absorption properties, making it a sought-after material for various applications [12, 16, 17]. However, it also has certain limitations, such as poor mechanical properties, rapid degradation, and uncontrolled swelling in aqueous environments [13].

© 2026 The Author(s). Published by IOP Publishing Ltd

In parallel with chitosan-based systems, other polymer matrices such as poly(vinyl alcohol) (PVA) and poly (ethylene oxide) (PEO) have attracted considerable attention due to their excellent film-forming ability, flexibility, and tunable optical properties. In particular, the incorporation of inorganic and magnetic nanofillers into PVA- and PEO-based polymers has been shown to effectively tailor their structural, optical, and optoelectronic characteristics. Mamand *et al* demonstrated that the insertion of black iron (III) oxide (Fe_2O_3) nanoparticles into a PEO matrix leads to a pronounced reduction in optical band gap energy, accompanied by significant modifications in the structural, magnetic, and optical properties of the resulting nanocomposites, highlighting their suitability for optoelectronic and magnetic device applications [18]. Similarly, Khasraw *et al* reported enhanced structural integrity and improved optical performance in PEO-based nanocomposites through nanoparticle incorporation, emphasizing the role of polymer–nanofiller interactions in governing electronic transitions and optical dispersion behavior [19].

Moreover, PVA-based nanocomposites doped with magnetic Fe_3O_4 nanoparticles have been shown to exhibit notable improvements in optical absorption, refractive index, and optoelectronic response. Recent work by Khasraw *et al* revealed that PVA:Fe_3O_4 magnetic nanocomposite films possess tunable optoelectronic characteristics, making them promising candidates for applications in optical sensors, photonic devices, and energy-related technologies [20]. These studies clearly demonstrate that polymer nanocomposites based on PVA and PEO provide versatile platforms for modulating optical and electronic properties, thereby offering a valuable framework for contextualizing the present CS/PVP-GnP system within the broader field of advanced polymer nanocomposites.

The standalone use of chitosan (CS) and polyvinylpyrrolidone (PVP) is often limited by poor mechanical strength, rapid degradation, and suboptimal optical properties. Both PVP and CS are water-soluble and biocompatible polymers [10], characteristics that make their combination particularly attractive for biomedical applications. PVP enhances the hydrophilicity of chitosan, facilitating the development of composites with improved water absorption capabilities [21]. Additionally, the film-forming ability of PVP complements that of chitosan, leading to the formation of more uniform and functionally effective films.

Carbon-based nanomaterials such as graphene and carbon nanotubes (CNTs) are widely employed to overcome the intrinsic limitations of polymers and to develop advanced nanocomposite materials with enhanced performance. Both graphene and CNTs exhibit exceptional mechanical, electrical, and optical properties, making them highly effective functional fillers in polymer matrices [10, 22–24]. Beyond chitosan- and PVP-based systems, graphene and graphene oxide (GO) have also been extensively incorporated into other polymer matrices to tailor their optical and optoelectronic properties. For instance, recent studies have shown that embedding GO into poly(vinyl alcohol) (PVA) significantly modifies the structural and morphological characteristics of the polymer while inducing pronounced changes in both linear and nonlinear optical behavior. In particular, varying GO concentrations in PVA films were found to reduce the optical band gap, enhance the refractive index, and improve nonlinear optical parameters, underscoring the effectiveness of graphene-based fillers in tuning optoelectronic performance across different polymer systems [25]. Such findings highlight the versatility of graphene-derived nanofillers and provide a meaningful framework for comparing graphene-reinforced PVA systems with the present CS/PVP-GnP nanocomposites. Owing to its two-dimensional structure and high surface area, graphene acts as an efficient reinforcing agent, while CNTs primarily contribute to improvements in mechanical strength and electrical conductivity. Consequently, the incorporation of graphene or CNTs into polymer matrices, including chitosan-based systems, has been consistently reported to enhance the optical, electrical, thermal, and mechanical properties of the resulting nanocomposites [10, 23].

Aziz *et al* demonstrated that the chitosan (CS) biopolymer, modified with natural dyes derived from hollyhock flower waste (HFW) in an environmentally sustainable manner, exhibits overall enhancement in optical properties, making it a promising candidate for optoelectronic applications [7]. Sarhan *et al* conducted a study that serves as a valuable reference for the preparation of silver (Ag)-doped chitosan (CS) nanocomposites intended for optoelectronic and biomedical applications [26]. In another study, the incorporation of multi-walled carbon nanotubes (MWCNTs) into a CS/PVA hybrid matrix resulted in the formation of hydrogels with tunable optical properties, positioning them as strong candidates for use in photonic devices, optical sensors, and optoelectronic systems [27]. Mamand *et al* also demonstrated that natural dyes extracted from waste flowers can offer an innovative and sustainable approach to enhancing the optoelectronic performance of chitosan-based biopolymers [28].

In this study, nanocomposite films were fabricated by incorporating graphene nanoplatelets (GnPs) into chitosan (CS) and poly(vinylpyrrolidone) (PVP) blends at varying ratios. The films were deposited onto quartz glass substrates using the spin-coating technique. The surface morphology and dispersion of GnPs within the polymer matrix were examined by scanning electron microscopy (SEM). Electrical conductivity was evaluated using standard conductivity measurements. Optical properties were investigated by UV–Vis spectroscopy, from which absorbance (A), reflectance (R), extinction coefficient (k), optical band gap energy (E_g), and Urbach energy (E_u) were determined using established models. The refractive index (n), optical conductivity

(σ_{opt}), and dielectric parameters were calculated based on the obtained optical data. In addition, linear and nonlinear optical parameters, including optical susceptibilities ($\chi^{(1)}$, $\chi^{(3)}$) and nonlinear refractive index (n_2), were evaluated using appropriate theoretical models.

2. Material and method

2.1. Materials

Deacetylated chitin, Poly(D-glucosamine) (448869 Sigma-Aldrich), hydrophilic polycarboxylate functionalized graphene nanoplatelets (806625 Sigma-Aldrich), poly(vinyl pyrrolidinone) (773417 Sigma-Aldrich) and acetic acid (A6283 Sigma-Aldrich) were purchased from Sigma Aldrich. The solvent used was a mixture of 1% acetic acid and double distilled water. Quartz glasses, transparent to UV light and measuring 2.5 × 2.5 cm^2, were used as the substrate for coating the films. All analytical chemicals were used without any further purification.

2.2. Preparation of PVP/GnP nanocomposite films

The CS/PVP-GnP nanocomposite films were prepared using the spin coating method. The CS/PVP (80/20 wt%) blend solution was prepared by mixing 1.44 g of CS and 0.36 g of PVP in 60 ml of a 1% acetic acid and double distilled water. The CS/PVP solution was stirred for 24 h at 50 °C. The obtained CS/PVP solution was transferred equally into six bottles. Then, the required amount of GnPs for the filler levels (0.00, 0.95, 2.12, 3.59, and 5.47 vol%) was added to each sample under magnetic stirring. After stirring the mixture for 140 h and sonicating it for 1 h, a homogenous GnP dispersion was obtained. Nanocomposite thin films were by dropping the resulting CS/PVP-GnP solutions onto vacuum fixed quartz glasses on the spin coater rotating at 1000 rpm. To ensure homogeneity, the prepared films were annealed at 80 °C for 2 h. A photograph of the obtained CS/PVP-GnP films is shown in figure 1(a). Film thicknesses were recorded at five different positions using a digital micrometer, and the average thicknesses were measured to be in the range of 25 ± 1.41 to 35 ± 0.71 μm.

2.3. Measurements

All measurements were performed using three identical composite films for each GnP volume fraction (ϕ) to ensure reproducibility. During all measurements, the laboratory temperature was maintained at 24 °C–25 °C and the relative humidity was controlled within the range of 55%–60%. The electrical resistivities of the CS/PVP-GnP nanocomposite films were measured in accordance with the ASTM D257 standard using a Keithley Model 6517 A electrometer. A custom-designed test fixture, based on a scaled-down configuration of the Keithley Model 8009 resistivity test fixture and equipped with disk-shaped electrodes, was employed [29]. After placing the composite films between the electrodes, electrical measurements were conducted using the alternating polarity method to minimize polarization and contact resistance effects. A DC voltage in the range of 50–100 V was applied, and the current response was recorded at 15 s intervals for each polarity. Electrical conductivity values were calculated from the measured resistance data, taking into account the sample geometry. For each composition, measurements were performed along three different orientations, and all measurements were repeated multiple times to reduce experimental uncertainty associated with surface resistance. The reported conductivity values represent the averaged results. Optical absorbance and reflectance spectra were recorded using a Varian Cary 100 Bio UV–Visible spectrophotometer (Varian Instruments, Australia) over the wavelength range of 200–600 nm. A scanning electron microscope, (SEM Zeiss Evo LS 10), was used to investigate the surface morphology of the CS/PVP-GnP nanocomposite film with 5.47 vol%.

3. Results and discussion

3.1. Scanning electron microscopy (SEM) analysis

Figure 1(b) shows a scanning electron microscope micrograph (SEM) of the CS/PVP-GnP composite with a volume fraction of 5.47 vol%. The image reveals that the GnPs are randomly distributed in the CS/PVP hybrid matrix. The shape and distribution of GnPs within the CS/PVP hybrid matrix play a crucial role in determining the nanocomposite's physical properties. From the figure, a GnP plate resembling a spherical form can be clearly observed, along with numerous GnPs in contact with each other surrounding it.

3.2. Electrical conductivity

As shown in table 1, the electrical conductivity of the composite materials obtained by adding GnP to the CS/PVP hybrid structure is significantly increased. The measured electrical conductivity value is 1.6×10^{-7} $S.m^{-1}$ for the pure CS/PVP hybrid, increasing to 28.6 $S.m^{-1}$ for the CS/PVP-GnP nanocomposite film with

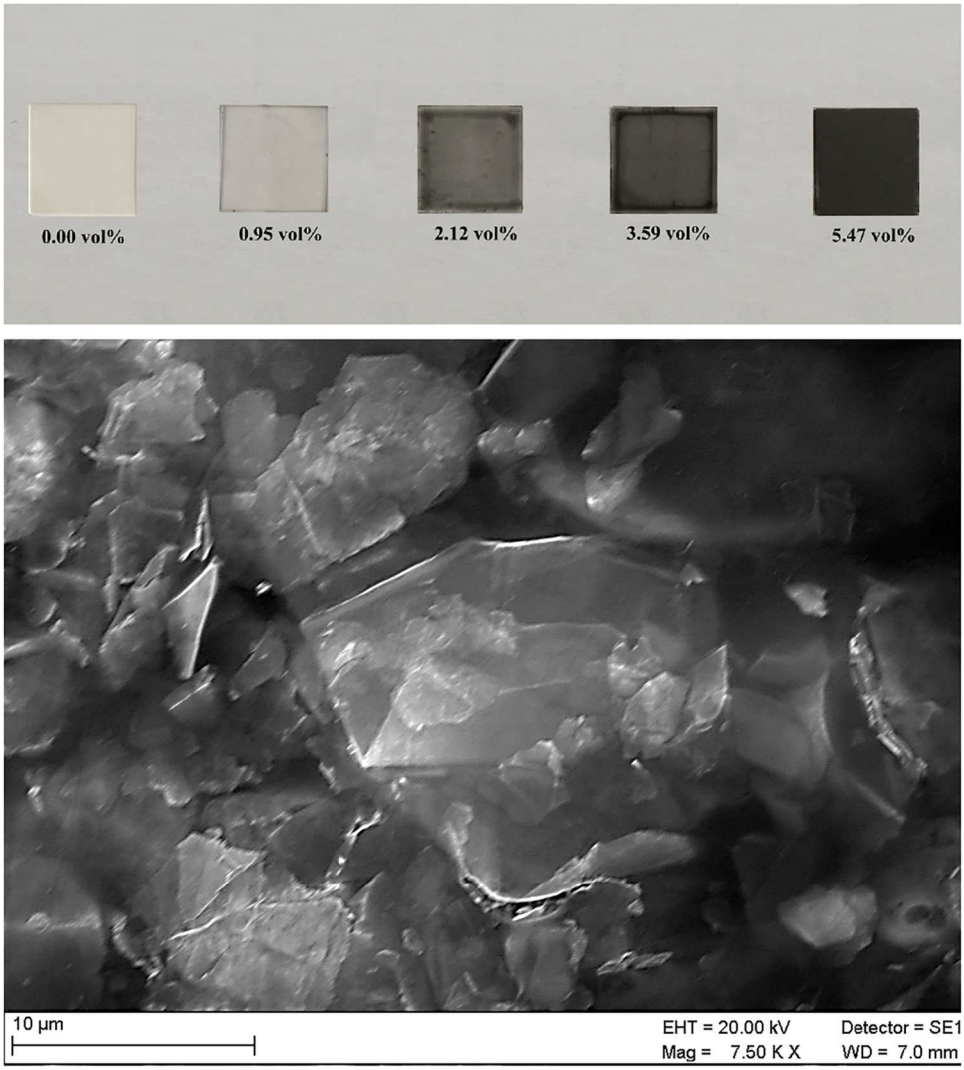

Figure 1. (a) The photograph image of CS/PVP-GnP nanocomposite films. (b) SEM image of CS/PVP-GnP nanocomposite film with $\phi = 5.47$ vol%.

Table 1. Electrical conductivity (σ), refractive index (n), Urbach energy (E_u) and optical band gap energies (E_g^d and E_g^i) for pure CS/PVP and CS/PVP-GnP nanocomposites.

ϕ (vol%)	σ (S m^{-1})	n (at 400 nm)	ASF method		
			E_g^d (eV)	E_g^i (eV)	E_u (eV)
0.00	1.6×10^{-7}	1.70	5.85	5.27	0.26
0.95	7.5×10^{-6}	1.72	5.80	5.01	0.47
2.12	0.8	1.76	5.68	4.49	0.80
3.59	5.2	1.82	5.58	4.00	1.24
5.47	28.6	1.87	5.32	3.08	1.96

5.47 vol% GnP. This enhancement is attributed to the much higher electrical conductivity of GnPs compared to the CS/PVP hybrid. When the GnPs are dispersed in the CS/PVP blend matrix, they form a conductive network with interconnected pathways, resulting in a significant increase in the conductivity of the composite. CS/PVP-GnP nanocomposites exhibit substantially higher conductivity than the pure CS/PVP matrix.

3.3. UV–vis analysis

The investigation of the UV–vis absorption spectrum is particularly useful for studying crystalline and amorphous polymeric materials, as it provides insight into their optical behavior, optical parameters, and electronic band structure [24, 30]. Figure 2 shows the absorbance (A) spectra of the pure CS/PVP hybrid matrix

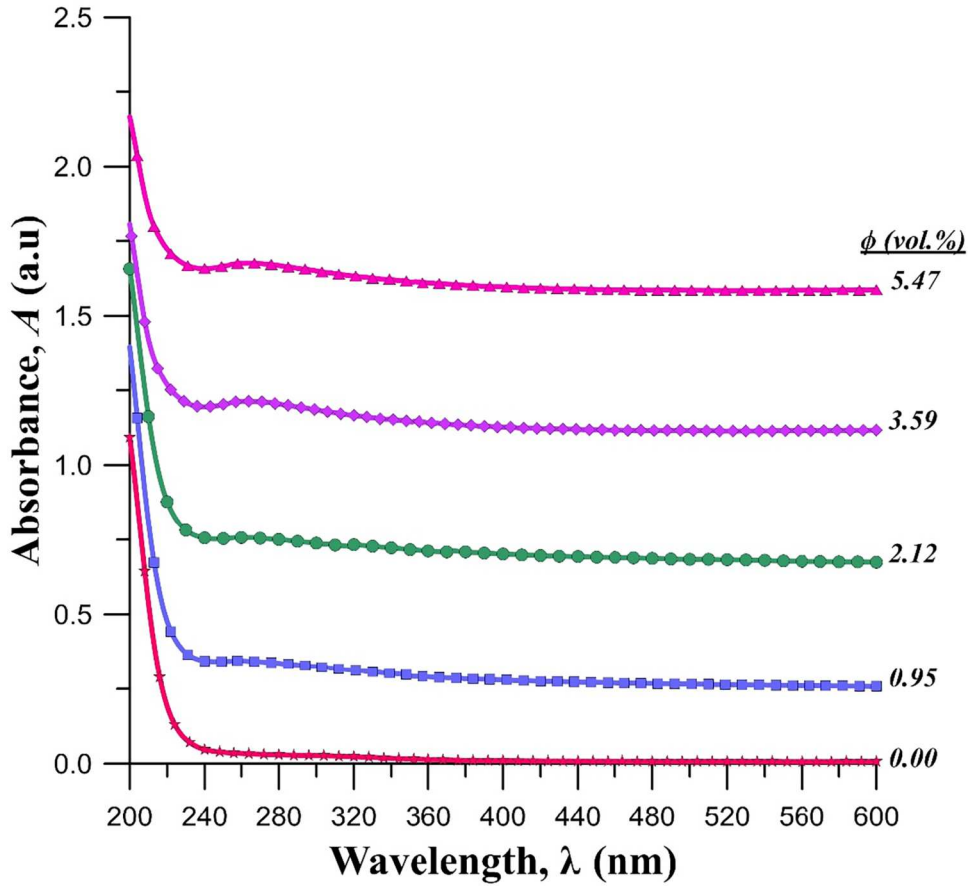

Figure 2. The Absorbance (A), spectra of pure CS/PVP hybrid matrix and CS/PVP-GnP nanocomposite films.

and CS/PVP-GnP nanocomposites in the wavelength range of 200–600 nm. The pure CS/PVP hybrid matrix exhibits low absorbance values across this range, indicating its transparency. Moreover, the CS/PVP-GnP nanocomposite films exhibit strong absorption in the 200–360 nm range while absorbance value remains almost constant across the 360–600 nm range. Absorbance values clearly increase with decreasing wavelength for all samples, especially below 360 nm. The figure also reveals that increasing the amount of GnP in the composites leads to higher absorbance levels. Additionally, a strong absorbance peak associated with the $\pi \rightarrow \pi^*$ transition is observed at approximately 200 nm [26, 28]. As the GnP content in the composites increases, the absorbance values rise notably, and the peak around 260 nm becomes more pronounced. This effect is due to the GnPs in the composite structure acting as photon scattering centers.

The absorption coefficient (α) is a fundamental optical parameter used to describe light attenuation in materials and allows meaningful comparison between films of different thicknesses. In this study, α was calculated from the absorbance (A) spectra using the film thickness (d) according to the following relation [31]:

$$\alpha = \frac{(2.303)A}{d} \tag{1}$$

The wavelength dependent absorption coefficient spectra of the pure CS/PVP hybrid matrix and CS/PVP-GnP nanocomposites, calculated from the absorbance data, are provided in the Supplementary Information (figure S1).

Similarly, the extinction coefficient (k), which represents optical losses associated with absorption and scattering processes and is relevant for photonic applications [32, 33], was determined from the absorption coefficient and wavelength (λ) using the following expression [31]:

$$k = \frac{\alpha\lambda}{4\pi} \tag{2}$$

The corresponding variation of the extinction coefficient with wavelength for the pure CS/PVP matrix and CS/PVP-GnP nanocomposites is presented in the Supplementary Information (figure S2). From this figure, it can be seen that the extinction coefficient (k) increases linearly in the high-wavelength (visible) region, whereas it decreases in the low-wavelength (UV) region, consistent with our previous study [30]. As the GnP volume

fraction in the composites increases, the absorption coefficient values also increase, leading to energy loss [34]. With higher GnP volume fractions in the CS/PVP composites, both the absorption coefficient and extinction coefficient values increase significantly. This indicates that the nanocomposites have an enhanced capacity to absorb and lose electromagnetic energy, suggesting that the absorption and extinction properties improve with increasing GnP concentration.

3.4. Determination of optical band gap energy

The energy difference between the highest occupied molecular orbital (HOMO) and the lowest unoccupied molecular orbital (LUMO) is referred to as the optical band gap (E_g) [30], which is a key parameter governing the optoelectronic behavior of polymer nanocomposites. In semiconductor systems, E_g can be estimated from optical absorption data using different formalisms, including the well-established Tauc relation, which correlates the absorption coefficient with photon energy according to:

$$\alpha h\nu = B(h\nu - E_g)^m \tag{3}$$

where α is the absorption coefficient, $h\nu$ is the photon energy, B is a constant, and m denotes the nature of the electronic transition ($m = 0.5$ for allowed direct and $m = 2$ for allowed indirect transitions).

In the present work, the optical band gap energies of the CS/PVP hybrid matrix and CS/PVP-GnP nanocomposites were determined using the absorption spectrum fitting (ASF) method, which directly utilizes absorbance data and minimizes uncertainties associated with film thickness measurements. Within the ASF framework, equation (3) can be rewritten in terms of absorbance as follows [34]:

$$A = C\lambda\left[\frac{1}{\lambda} - \frac{1}{\lambda_g}\right]^m + D \tag{4}$$

where A represents absorbance, λ is the wavelength, λ_g corresponds to the wavelength associated with the optical band gap energy, m indicates the type of electronic transition, and C and D are fitting constants.

For the CS/PVP hybrid matrix and CS/PVP-GnP nanocomposites, the $(A\lambda^{-1})^{\frac{1}{m}}$ versus λ^{-1} graphs for direct and indirect transitions are plotted in figures 3(a) and (b), respectively. The λ_g values are determined by extrapolating the linear region to λ^{-1} axis, as shown in figures 3(a) and (b). The band gap energies corresponding to λ_g were calculated using the equation below and are presented in table 1.

$$E_g = \frac{1239.83}{\lambda_g} \tag{5}$$

For the pure CS/PVP hybrid matrix, the direct and indirect optical band gap energies were found to be 5.86 eV and 5.27 eV, respectively. With increasing GnP volume fraction, a systematic reduction in E_g was observed. In particular, for the nanocomposite containing $\phi = 5.47$ vol% GnPs, the direct and indirect band gap energies decreased to 5.32 eV and 3.06 eV, respectively.

The observed reduction in optical band gap energy with increasing GnP content is attributed to the formation of charge-transfer complexes and the introduction of localized electronic states within the forbidden band, which facilitate electronic transitions at lower photon energies [31]. This interpretation is further supported by the inverse correlation between optical band gap energy and electrical conductivity shown in figure 4, where the enhancement in conductivity accompanies the narrowing of E_g due to increased charge carrier density in the nanocomposite system.

3.5. Determination of urbach energy

The Urbach energy (E_u) is an important parameter that characterizes the degree of structural disorder and defect states within the band gap of semiconductors and amorphous materials. It is associated with the exponential absorption tail, known as the Urbach tail, which originates from localized electronic states near the band edges and reflects the presence of defects and lattice imperfections in the material [34]. The analysis of Urbach energy provides valuable insight into structural disorder, defect density, and localized states, which are critically important for the performance of photovoltaic, optoelectronic, and semiconductor devices [24]. The Urbach energy is related to the photon energy through the following expression [24]:

$$\alpha = \alpha_0 \exp\left(\frac{h\nu}{E_u}\right) \tag{6}$$

In equation (6) where α_0 is a pre-exponential constant. In addition to the conventional formulation based on the absorption coefficient, the Urbach energy can be reliably determined using absorbance data via the Absorption Spectrum Fitting (ASF) approach. In this method, equation (6) can be rewritten as [34]:

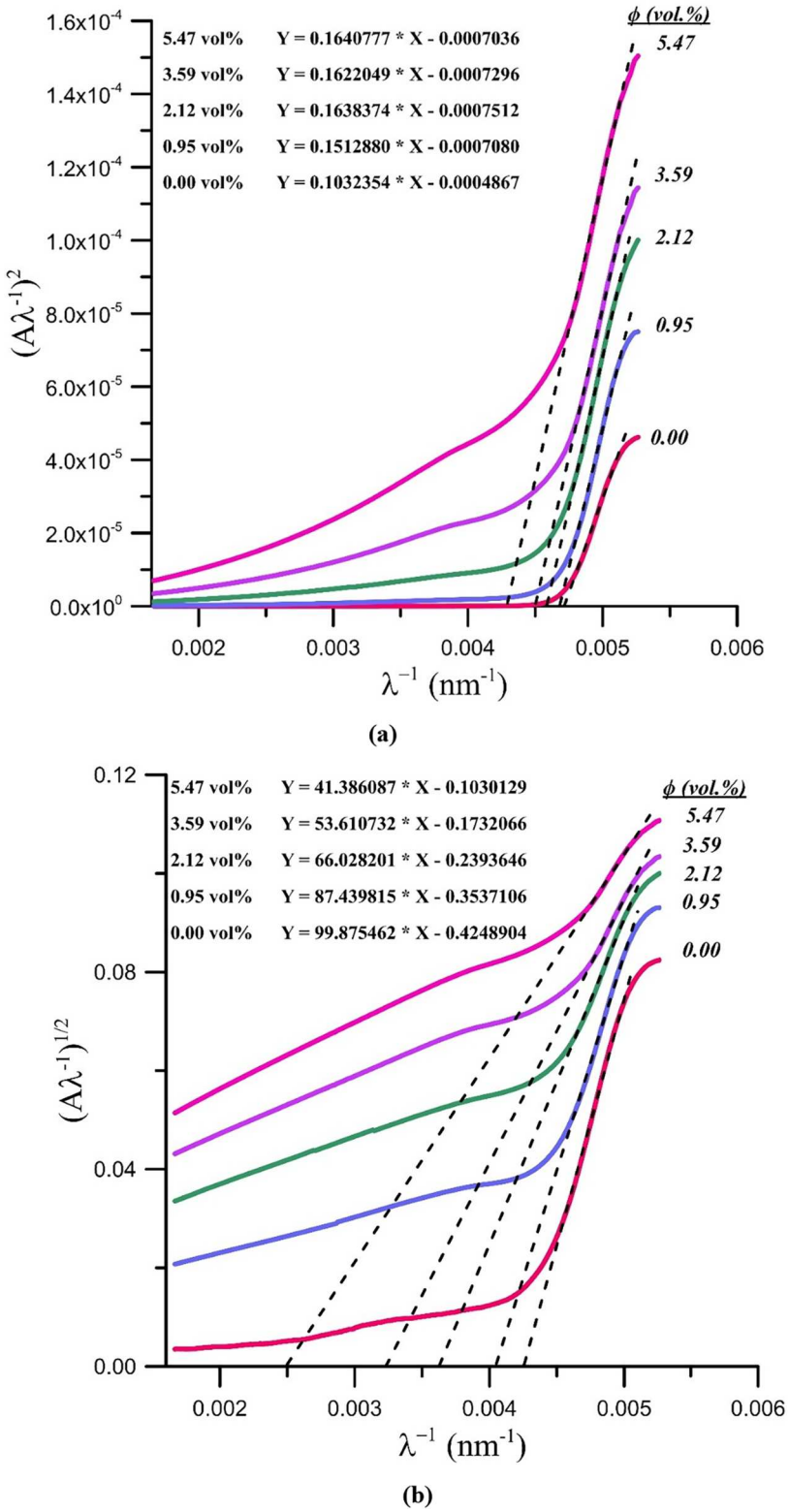

Figure 3. (a) $(A\lambda^{-1})^2$ versus (λ^{-1}) plot and (b) $(A\lambda^{-1})^2$ versus (λ^{-1}) plot of pure CS/PVP hybrid matrix and CS/PVP-GnP nanocomposites.

$$A = F \exp\left(\frac{hc}{E_u \lambda}\right) \tag{7}$$

where F is a constant. The E_u values of CS/PVP-GnP nanocomposites according to ASF method were determined from the slope of the linear part of the $ln(A)$ versus $(1/\lambda)$ plots shown in figure 5, using the formula $E_u = 1239.83/\text{slope}$, and are presented in table 1.

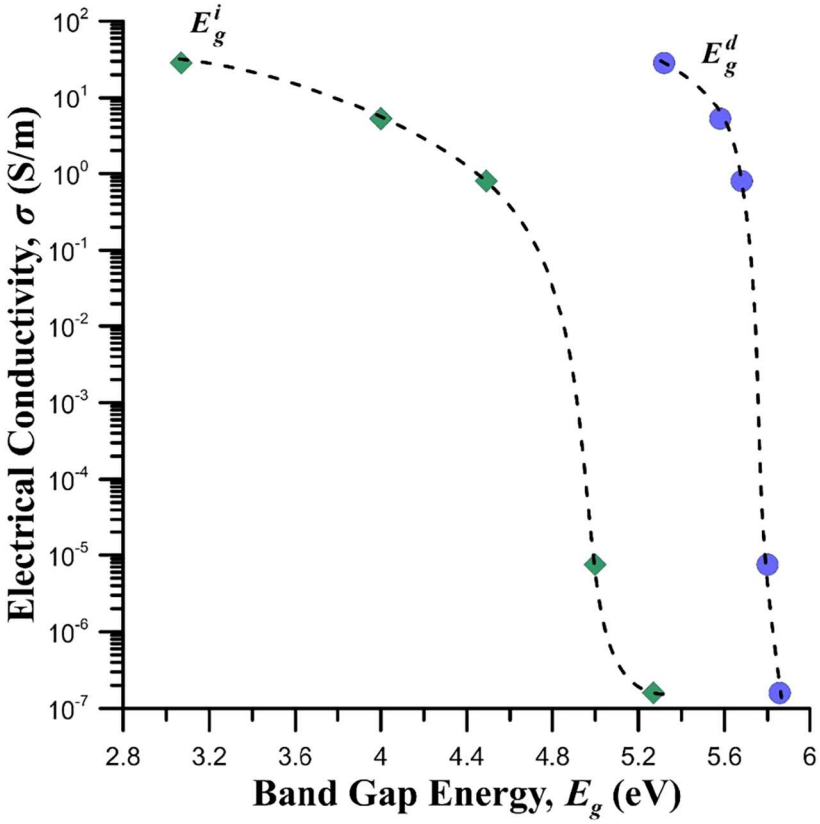

Figure 4. Electrical conductivity (σ) of CS/PVP-GnP nanocomposites versus optical band gap energies (E_g^d and E_g^i).

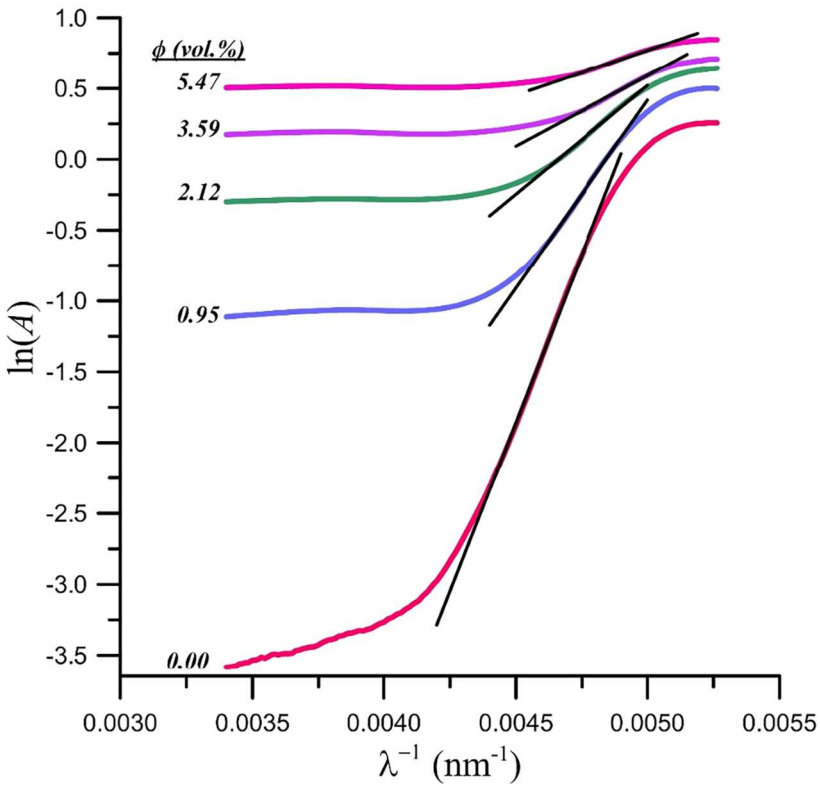

Figure 5. (ln A) versus (λ^{-1}) plots of pure CS/PVP hybrid matrix and CS/PVP-GnP nanocomposites.

As presented in table 1, the Urbach energy of the pure CS/PVP hybrid matrix was found to be 0.26 eV and increased progressively with increasing GnP content, reaching a maximum value of 1.96 eV at 5.47 vol% GnP. This systematic increase in E_u indicates an enhanced degree of structural disorder and a higher density of localized defect states within the forbidden band, which can facilitate electronic transitions in the nanocomposite system [35].

3.6. Reflectance (*R*) and refractive index (*n*)

The optical reflection spectra of the pure CS/PVP hybrid matrix and CS/PVP-GnP nanocomposites are given in figure 6(a). It is seen from the figure that the reflectance values of both pure CS/PVP hybrid matrix and CS/PVP-GnP nanocomposites vary with wavelength and remain almost constant above 400 nm. The CS/PVP-GnP nanocomposites exhibit higher reflectance values compared to the pure CS/PVP hybrid matrix. Furthermore, the increase in reflectance values correlates with higher GnP content, as GnPs act as a reflective phase within the nanocomposites.

The refractive index (n) is a fundamental parameter for evaluating the optical properties of a material and represents the ratio of the speed of light in the vacuum to its speed within the material. This physical parameter is critically important for various applications, including the fabrication of optoelectronic devices, the selection of anti-reflective materials, and the design of optical filters and integrated devices [36, 37]. The refractive index determines the optical behavior of a material by influencing light propagation, reflection, and absorption coefficients. Fillers such as nanoparticles can increase the refractive index by enhancing the density of composite films. The refractive index was calculated using the equation below, incorporating reflection (R) and extinction coefficient (k) [31].

$$n = \left(\frac{1+R}{1-R}\right) + \sqrt{\frac{4R}{(1-R)^2} - k^2} \tag{8}$$

The variation of n values of pure CS/PVP hybrid matrix and CS/PVP-GnP nanocomposites with wavelength is shown in figure 6(b). As can be seen from the figure, the refractive index remains almost constant in the visible region for all samples, while a rapid and significant increase in n values is observed when the wavelength decreases below 400 nm. The calculated refractive index values for $\lambda = 400$ nm are presented in table 1 for all samples. Table 1 shows that the refractive index values of the nanocomposites increase with the incorporation of GnP nanoparticles into the CS/PVP hybrid matrix.

An increase in filler concentration affects the internal structure of the polymer, leading to a rise in the refractive index. This increase results from the use of a filler with a different density than the polymer and alterations in the matrix structure [36, 38]. The addition of GnPs to the hybrid structure modifies the packing density of the mixture, causing variations in the refractive index. Furthermore, GnP incorporation introduces new defects into the composite matrix, influencing the density and polarizability of the structure [39, 40]. These effects reduce the light transmission rate through the polymer and explain the increase in refractive index with increasing filler concentration [38]. The wavelength-dependent real and imaginary parts of the dielectric constant, calculated from the refractive index and extinction coefficient, are provided in the Supplementary Information (Section S1.2).

3.7. Optical conductivity

The interaction of electromagnetic radiation with a material can excite the material electrons across the bandgap, thereby enhancing its electrical and optical conductivity; this phenomenon is referred to as photoconductivity and plays a crucial role in determining the optoelectronic properties of the material [36, 41]. Optical conductivity (σ_{opt}) represents the material's optical response to electromagnetic waves and is closely associated with interband optical transitions [42]. The reduction of factors such as crystal defects, stress, and lattice deformations improves conductivity, enabling faster propagation of electromagnetic waves and freer movement of electrons within the material [43]. Furthermore, optical conductivity, which depends on the material's absorption coefficient and refractive index, serves as a fundamental parameter for analyzing the optical properties and atomic structure of solids. It is mathematically expressed by the following equation [28, 31].

$$\sigma_{opt} = \frac{\alpha n c}{4\pi} \tag{9}$$

In this equation, c is the speed of light in vacuum. The variation of optical conductivity with wavelength for the pure CS/PVP hybrid matrix and CS/PVP-GnP nanocomposites is presented in figure 7. As shown in the figure, optical conductivity increases with decreasing wavelength. This can be explained by the fact that photons with shorter wavelengths have sufficient energy to excite electrons in the material more effectively. Since optical conductivity is directly proportional to the absorption coefficient, an increase in the absorption

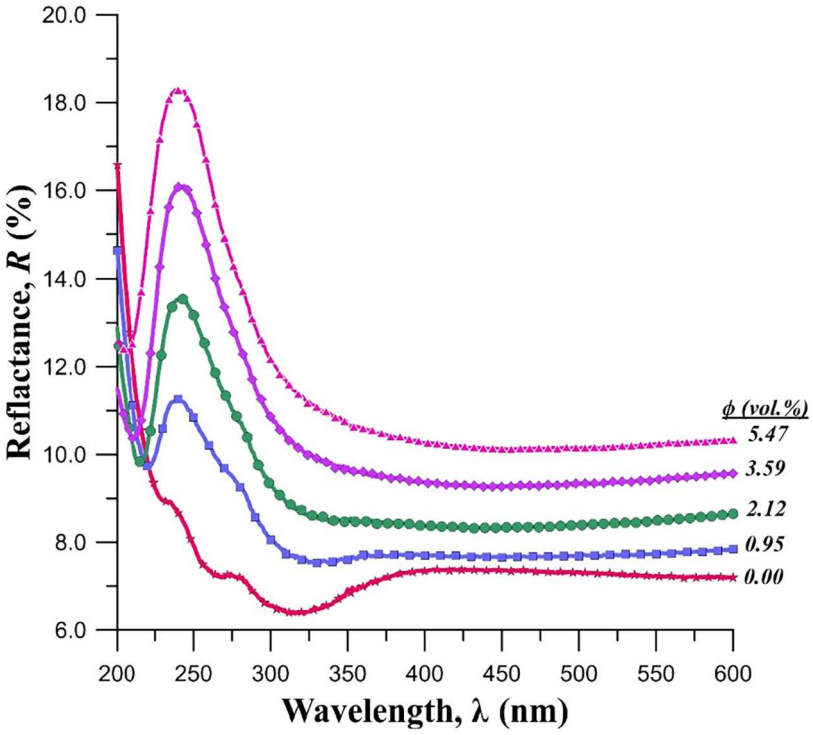

(a)

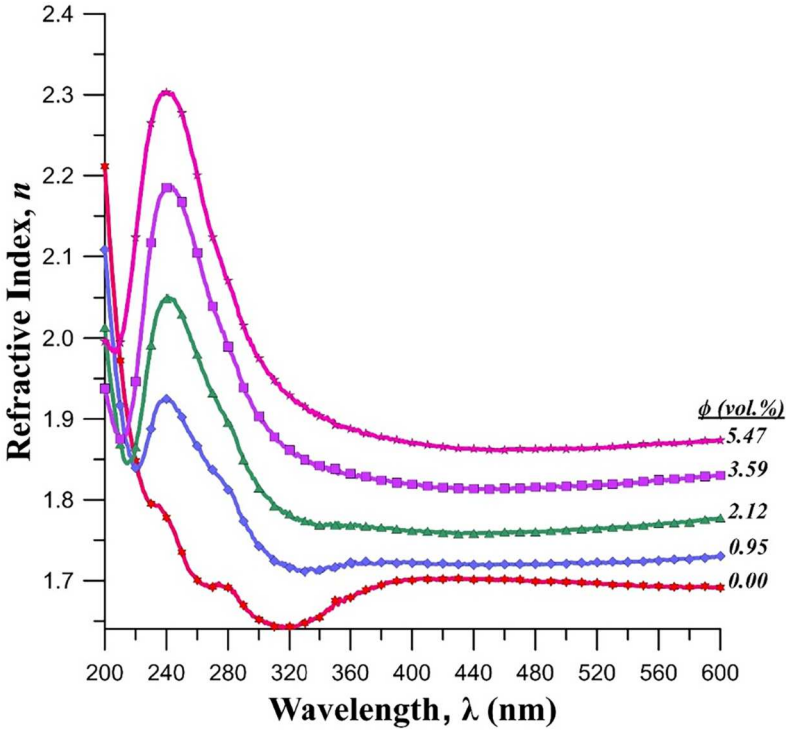

(b)

Figure 6. (a) The reflectance (R) and (b) The refractive index (n) spectra versus wavelength (λ) pure CS/PVP hybrid matrix and CS/PVP-GnP nanocomposites.

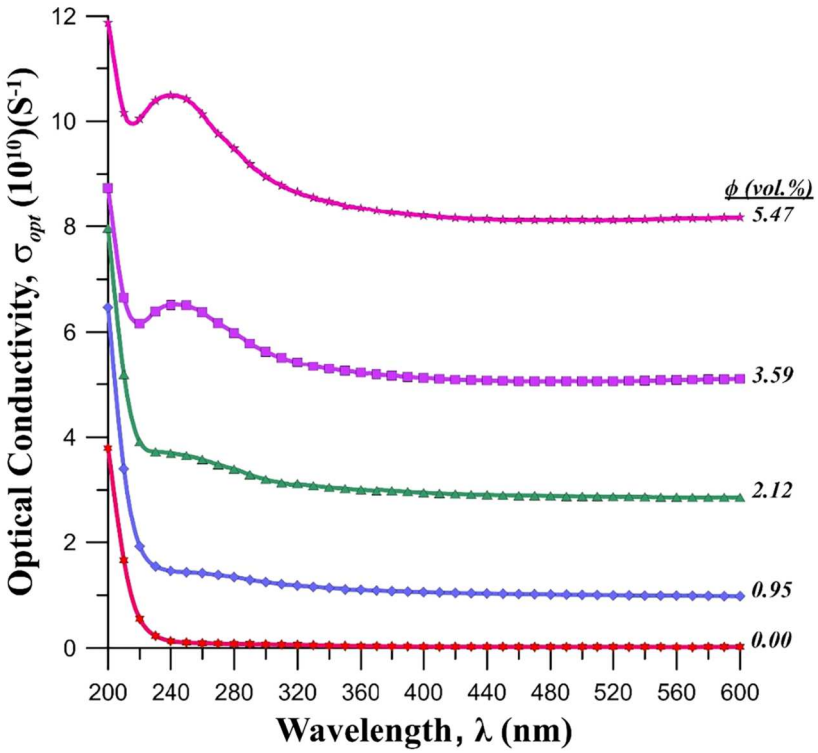

Figure 7. The optical conductivity (σ_{opt}) spectra versus wavelength (λ) for pure CS/PVP hybrid matrix and CS/PVP-GnP nanocomposites.

coefficient also leads to enhanced optical conductivity. In the low-wavelength region, photon energy is sufficient to excite electrons from the valence band to the conduction band, resulting in a significant increase in optical conductivity.

The addition of GnP nanoparticles increases the density of localized states within the energy range, thereby increasing the absorption coefficient and the optical conductivity of the nanocomposites [31]. This increase is associated with the formation of charge transfer complexes between GnP and the CS/PVP matrix and the increase in the number of free charge carriers due to doping. Furthermore, the decrease in the crystallinity of polymer films reduces the optical bandgap, contributing to higher optical conductivity. Structural irregularities and the increase in defect states facilitate electron mobility within the bandgap, further increasing optical conductivity [32, 41]. The high and stable σ_{opt} values, in the range of 10^{10} to 10^{11} S^{-1}, indicate that the films exhibit strong photo-response and have a potential for applications in optoelectronic devices [39].

3.8. Dispersion energy parameters

Dispersion energy parameters play a crucial role in understanding the optical behavior of materials and their interactions with light. They provide significant insights into the electronic structures of materials, especially when analyzed through single-oscillator models like the Wemple-DiDomenico (W-D) model [44, 45]. The W-D model finds extensive applications in fields such as optical material characterization, optical device design (e.g., filters, lenses, waveguides), photovoltaic applications, and dielectric/conductivity studies [33, 45–47]. It is particularly important in studying the optical properties of composite materials and nanostructures. The W-D model is a method used to investigate how a material's refractive index (n) changes with wavelength in the normal dispersion region, with the spectral dependence of the refractive index expressed by the following equation [47, 48]:

$$\frac{1}{n^2-1} = \frac{E_o}{E_d} - \frac{1}{E_o E_d}(h\nu)^2 \tag{12}$$

here, E_d and E_o represent the dispersion energy and oscillator energy, respectively. E_d includes the average density of interband optical transitions within the material and is closely related to the chemical bonding structure, charge distribution within the unit cell, and structural order of the material [28, 44, 47]. The E_d value provides information about the type and energy of chemical bonds and also indicates the changes in structural order and defect density within the material [28, 41, 42, 47, 49].

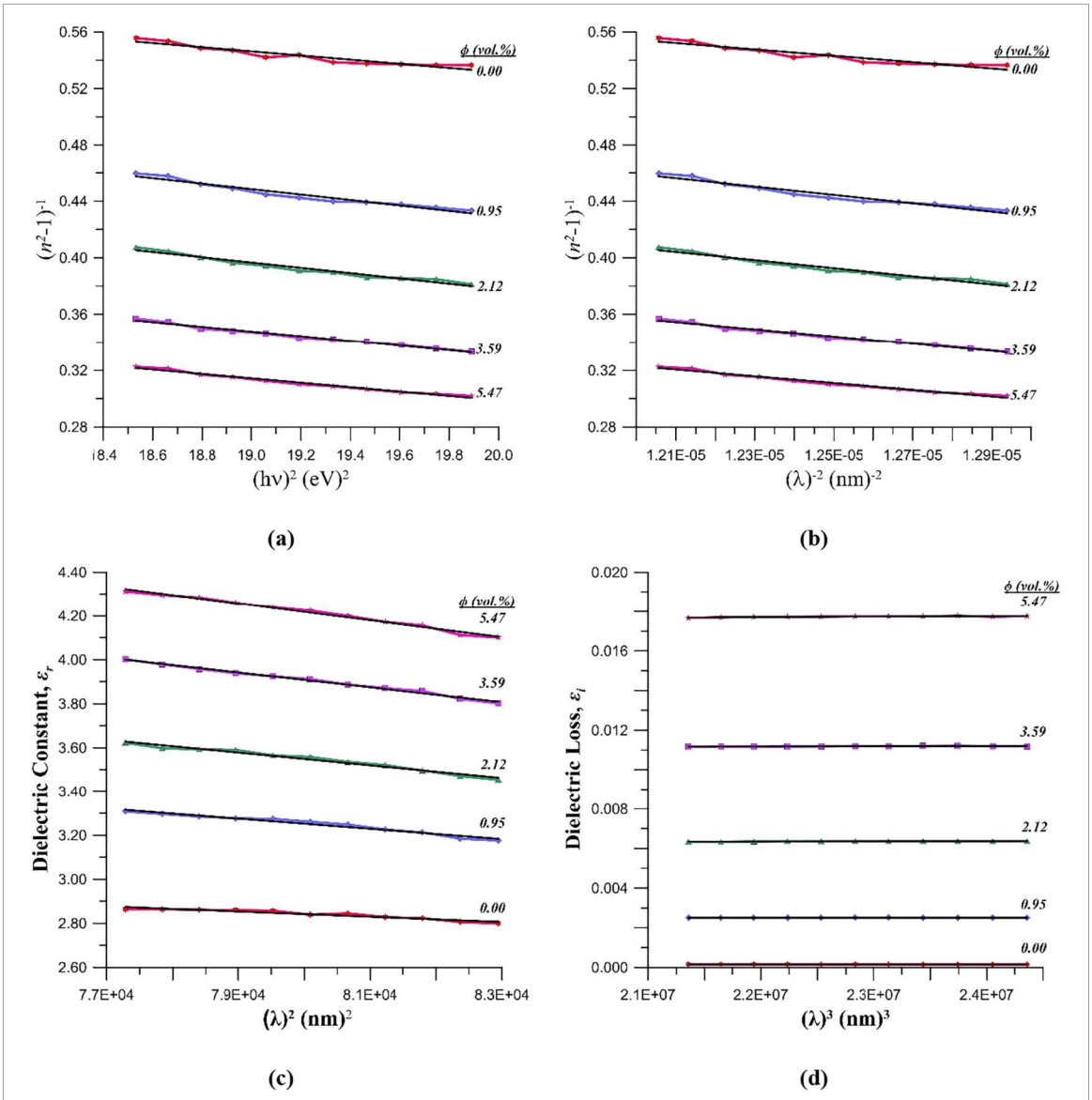

Figure 8. (a) Plots of $(n^2–1)^{-1}$ versus $(h\nu)^2$, (b) Plots of $(n^2–1)^{-1}$ versus $(\lambda)^{-2}$, (c) Plots of (ε_r) versus $(\lambda)^2$ and (d) Plots of (ε_i) versus $(\lambda)^3$ of the pure CS/PVP hybrid matrix and CS/PVP-GnP nanocomposites.

On the other hand, E_o represents the average band gap energy of the material, also known as the forbidden band energy. This value depends on the composition and structure of the material and provides information about the overall band structure [28, 41, 42, 44, 47, 49]. As shown in figure 8(a), if plotting $(n^2 - 1)^{-1}$ versus $(h\nu)^2$, a linear relationship between the values in the graph is observed. From the slope and intercept of this line, E_o and E_d can be determined.

Additionally, using the W-D model, other optical constants of the material can also be determined, such as the static refractive index (n_∞), static dielectric constant (ε_s), and oscillator strength (f) [28, 49, 50].

$$n_o = \left(1 + \frac{E_d}{E_o}\right)^{1/2} \tag{13}$$

$$\varepsilon_s = (n_\infty)^2 \tag{14}$$

$$f = E_d E_o \tag{15}$$

The calculated values of E_d, E_o, n_∞, ε_s, f, and E_o/E_g^d for the pure CS/PVP hybrid matrix and CS/PVP-GnP nanocomposites are presented in table 2. The dispersion energy (E_d) exhibits a non-monotonic dependence on GnP volume fraction, decreasing from 9.09 eV for pure CS/PVP to 8.00 eV at $\phi = 0.95$ vol%, followed by an increase to 10.24 eV at $\phi = 5.47$ vol% GnP. This behavior cannot be explained solely by bandgap narrowing. Within the Wemple–DiDomenico framework, E_d reflects the strength of interband optical transitions and is sensitive to structural ordering and electronic polarizability. At low GnP content, increased interfacial disorder

Table 2. E_d, E_o, n_∞, ε_s, f, λ_o, S_o and E_o/E_g^d values of the pure CS/PVP and CS/PVP-GnP nanocomposites.

ϕ (vol%)	E_d (eV)	E_o (eV)	n_∞	ε_s	f(eV)^2	λ_o (nm)	S_o (10^{13}) (m^{-2})	E_o/E_g^d
0.00	9.09	7.50	1.48	2.21	68.17	165.25	4.44	1.28
0.95	8.00	6.50	1.49	2.23	52.00	190.60	3.38	1.12
2.12	8.44	6.34	1.52	2.33	53.50	195.46	3.48	1.11
3.59	9.48	6.30	1.58	2.50	59.72	196.50	3.89	1.13
5.47	10.24	6.25	1.62	2.64	64.00	198.11	3.83	1.18

and localized defect states reduce the effective oscillator strength, leading to a decrease in E_d. At higher GnP loadings, enhanced π–π interactions and improved electronic coupling between GnPs and the polymer matrix strengthen interband transitions, resulting in an increase in E_d despite the continued reduction in optical band gap [39, 45, 49]. The minimum E_d observed at $\phi = 0.95$ vol% corresponds to a transition regime rather than an optimized composition, whereas higher GnP contents provide enhanced electronic polarizability and refractive response. As shown in table 2, the E_o/E_g^d ratio varies between 1.11 and 1.28. The n_∞ corresponding to the material's refractive index at long wavelengths increased from 1.48 for pure CS/PVP to 1.62 for $\phi = 5.47$ vol% GnP. Similarly, ε_s increased from 2.21 for pure CS/PVP to 2.64 for $\phi = 5.47$ vol% GnP. In contrast to the ε_s, the f decreased from 68.17 for pure CS/PVP to 64.00 for $\phi = 5.47$ vol% GnP.

The Sellmeier oscillator model explains the relationship between the refractive index and wavelength based on oscillations arising from the interaction of light with atoms and molecules within the material [51]. The single-term Sellmeier model simplifies the equation by assuming that the lowest-energy oscillator contributes most significantly to the refractive index. This model describes the wavelength dependence of the refractive index using parameters such as the average oscillator strength (S_o) and the average oscillator wavelength (λ_o) [49, 52, 53]. The Sellmeier oscillator model is expressed by the following equation [49, 54]:

$$\frac{n_\infty^2 - 1}{n^2 - 1} = 1 - \left(\frac{\lambda_o}{\lambda}\right)^2 \tag{16}$$

here, n_∞ represents the static refractive index at long wavelengths, and λ_o denotes the medium oscillator wavelength. When the equation is rearranged with respect to equation (16), the following expressions are obtained:

$$(n^2 - 1)^{-1} = \frac{1}{S_o \lambda_o^2} - \frac{1}{S_o}\lambda^{-2} \tag{17}$$

$$S_o = \frac{n_\infty^2 - 1}{\lambda_o^2} \tag{18}$$

Here, S_o represents the average oscillator strength. From the slope of the graph plotting $(n^2 - 1)^{-1}$ against λ^{-2} in figure 8(b), the value of S_o^{-1} is determined, while the intercept on the Y-axis provides the value of $(S_o \lambda_o^2)^{-1}$. Using these values, the calculated average oscillator strength (S_o) and average oscillator wavelength (λ_o) are given in table 2. As shown in table 2, S_o decreases from 4.44×10^{13} m^{-2} for pure CS/PVP to 3.38×10^{13} m^{-2} for $\phi = 0.95$ vol% GnP, and then increases to 3.83×10^{13} m^{-2} $\phi = 5.47$ vol% GnP. Meanwhile, λ_o increases from 165.25 nm for pure CS/PVP to 198.11 nm for $\phi = 5.47$ vol% GnP.

The relationship between the real dielectric constant (ε_r) of nanocomposite materials and the wavelength (λ) can be analyzed using the Spitzer-Fan model. This model is particularly significant for understanding the behavior of free charge carriers in semiconductors [37, 44, 46]. The main idea of the model is that the dielectric response of a material is determined by the presence of free charge carriers and their interaction with the applied electromagnetic field [44, 45]. It is expressed by the following equation [45].

$$\varepsilon_r = n^2 - k^2 = \varepsilon_l - \left(\frac{e^2}{4\pi^2 c^2 \varepsilon_o}\frac{N}{m^*}\right)\lambda^2 \tag{19}$$

Here, ε_l, e, c, ε_o, and N/m^* represent the dielectric constant at short wavelengths, the electron charge, the speed of light, the permittivity of free space, and the ratio of charge carrier density (N) to the effective mass (m^*), respectively. From the graph of ε_r plotted against λ^2 in figure 8(c), the values of ε_∞ and N/m^* were determined and are given in table 3. For pure CS/PVP, $\varepsilon_l = 3.79$ and $N/m^* = 1.44 \times 10^{58}$ kg m^{-3}, which increase to $\varepsilon_l = 7.30$ and $N/m^* = 4.68 \times 10^{58}$ kg m^{-3}, for $\phi = 5.47$ vol% GnP. The increase in ε_l and N/m^* values is associated with an increase in the number of free charge carriers, indicating a greater contribution to the polarization mechanism of the material [37, 44–46].

The Drude free electron model is very important for understanding the collective behavior and interactions of free electrons within a material. Using this model, it is possible to determine various key parameters, such as

Table 3. ω_p μ_{opt}, τ, ε_l, and N/m^* values of the pure CS/PVP and CS/PVP-GnP nanocomposites.

ϕ (vol%)	ω_p (10^{32}) (s^{-1})	μ_{opt} (10^{-1}) ($C\,s\,kg^{-1}$)	τ (10^{-12}) (s)	ε_l	N/m^* (10^{58}) ($kg\,m^{-3}$)
0.00	0.42	7.85	5.17	3.79	1.44
0.95	0.82	1.71	11.3	5.11	2.82
2.12	1.02	3.69	2.4	5.86	3.51
3.59	1.19	4.04	2.6	6.60	4.10
5.47	1.35	2.03	1.3	7.30	4.68

the relaxation time (τ), optical electronic mobility (μ_{opt}), and resonant plasma frequency (ω_p). According to the model, the relationship between dielectric loss (ε_i) and wavelength (λ) is given by the following equation [44, 45].

$$\varepsilon_i = J\left(\frac{1}{\tau}\right)\lambda^3,\ J = \frac{e^2}{8\pi^3 c^3 \varepsilon_o}\frac{N}{m^*} \tag{20}$$

Figure 8(d) illustrates the variation of ε_i values for the pure CS/PVP hybrid matrix and CS/PVP-GnP nanocomposites as a function of λ^3. The relaxation time (τ) can be calculated using the slope of the straight lines in the figure according to equation (20). Additionally, the optical electronic mobility (μ_{opt}) and the resonant plasma frequency (ω_p) can be determined using the following equations [44, 45]:

$$\mu_{opt} = \frac{e\tau}{m^*} \tag{21}$$

$$\omega_p = \frac{e^2 N}{\varepsilon_o m^*} \tag{22}$$

The calculated values of τ, μ_{opt}, and ω_p for the pure CS/PVP hybrid matrix and CS/PVP-GnP nanocomposites are presented in table 3. For pure CS/PVP, $\tau = 5.17 \times 10^{-12}$ s and $\mu_{opt} = 7.85 \times 10^{-1}$, which decrease to $\tau = 1.3 \times 10^{-12}$ s and $\mu_{opt} = 2.03 \times 10^{-1}$ for $\phi = 5.47$ vol% GnP. Conversely, ω_p increases from 0.42×10^{32} s^{-1} for pure CS/PVP to 1.35×10^{32} s^{-1} for $\phi = 5.47$ vol% GnP. These changes confirm an increase in the number of free charge carriers in the nanocomposites.

3.9. Nonlinear optical properties

Nonlinear optical (NLO) polymer composites offer significant application potential in fields such as telecommunications, optical data storage, and information processing [39, 42]. These materials, which fulfill key criteria such as high durability, thermal stability, and transparency, play a critical role in advancing modern optical technologies [28]. Nonlinear optical (NLO) responsiveness is characterized by the polarization exhibited by materials in response to an electric field, and is defined by the following equation [35, 42]:

$$P = \chi^{(1)}E + \chi^{(2)}E^2 + \chi^{(3)}E^3 \tag{23}$$

Here, $\chi^{(1)}$ represents the linear susceptibility, while $\chi^{(2)}$ and $\chi^{(3)}$ denote the second- and third-order NLO susceptibilities, respectively [32]. These parameters are critical for understanding the optical behavior of materials, particularly in response to high-intensity laser pulses, and for their application in NLO device design [35]. The relationship between linear susceptibility $\chi^{(1)}$ and third-order nonlinear susceptibility $\chi^{(3)}$ can be described by the Miller rule, and these two parameters are fundamental to understanding a material's optical properties [49]. The direct proportionality between the refractive index (n) and linear susceptibility $\chi^{(1)}$ plays an important role in calculating more complex optical behaviors, such as the nonlinear refractive index (n_2). $\chi^{(1)}$, $\chi^{(3)}$, and n_2 can be determined using the following expressions [32, 36, 42, 49]:

$$\chi^{(1)} = \frac{n^2 - 1}{4\pi} \tag{24}$$

$$\chi^{(3)} = 1.7 \times 10^{-10}(\chi^{(1)})^4 \tag{25}$$

$$n_2 = \frac{12\pi}{n}\chi^{(3)} \tag{26}$$

Figures 9(a)–(c) illustrate the λ-dependent variations in $\chi^{(1)}$, and n_2 spectra for pure CS/PVP and CS/PVP-GnP nanocomposites. As the GnP content in the composites increases, $\chi^{(1)}$, $\chi^{(3)}$, and n_2 also increase. For instance, at 400 nm, the values for pure CS/PVP are $\chi^{(1)} = 0.15$ esu, $\chi^{(3)} = 8.7 \times 10^{-14}$ esu, and $n_2 = 1.9 \times 10^{-12}$, which increase to $\chi^{(1)} = 0.20$ esu, $\chi^{(3)} = 2.6 \times 10^{-13}$ esu, and $n_2 = 5.3 \times 10^{-12}$ for $\phi = 5.47$ vol% GnP. The incorporation of GnP into the polymer matrix significantly enhances the nonlinear optical properties by inducing

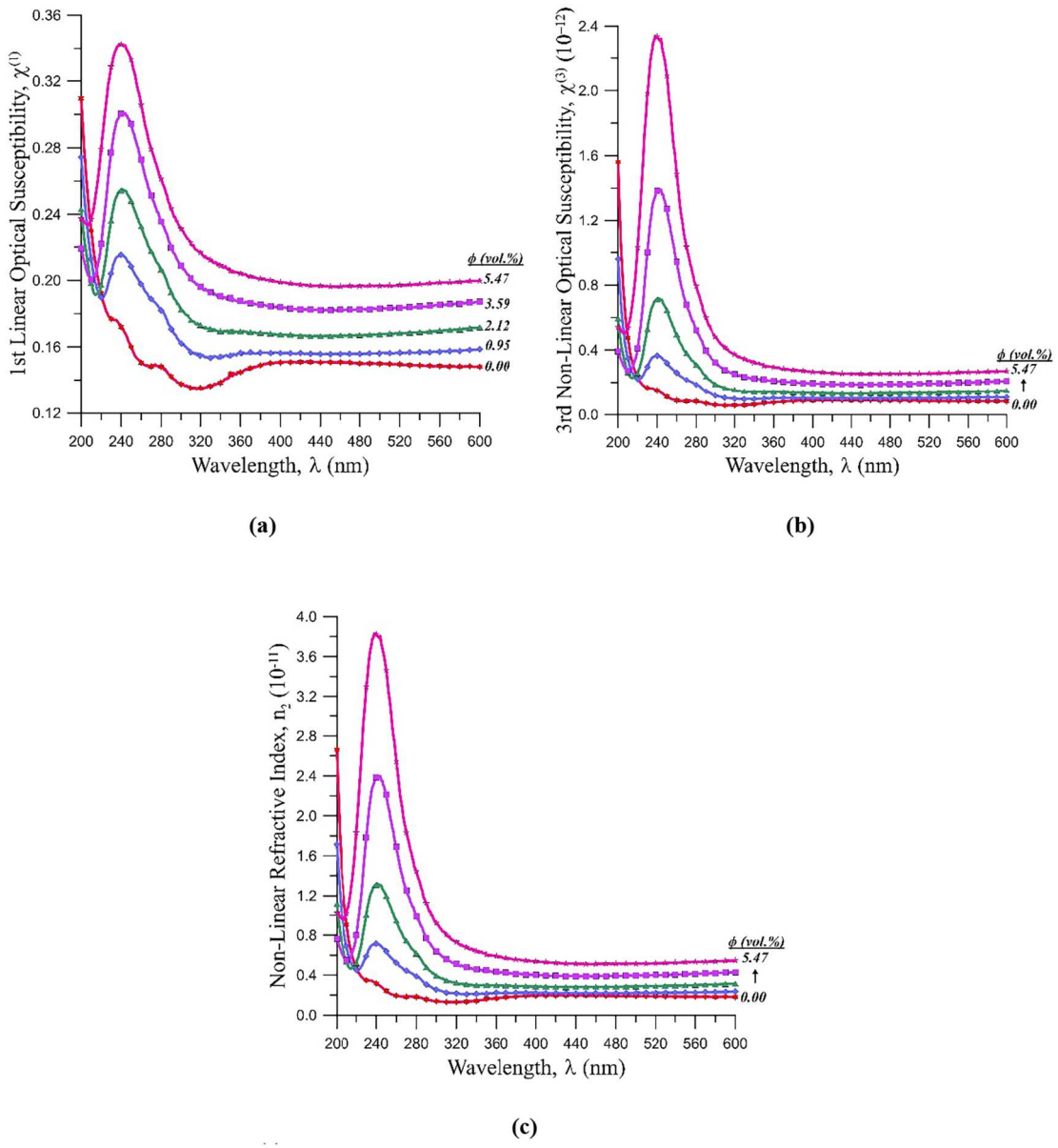

Figure 9. (a) ($\chi^{(1)}$), (b) ($\chi^{(3)}$) and (c) (n_2) versus the wavelength (λ) of the pure CS/PVP hybrid matrix and CS/PVP-GnP nanocomposites.

defect centers and increasing local polarizability of the composite. The strong interaction between GnP and the matrix further supports this enhancement by increasing the number of defects and energy carriers. These advancements in the NLO properties of CS/PVP-GnP nanocomposites position them as promising candidates for next-generation applications in communications, photonic devices, and optical switching.

4. Conclusions

In this study, CS/PVP-GnP nanocomposite thin films were fabricated via the spin-coating technique, and their structural, electrical, and optical properties were systematically examined as a function of GnP volume fraction. Electrical measurements revealed a pronounced increase in conductivity with increasing GnP content, indicating the formation of conductive networks within the polymer matrix. UV–Vis spectroscopy showed strong absorption in the ultraviolet region for all samples. The optical band gap, determined using the absorption spectrum fitting (ASF) method, decreased progressively with increasing GnP loading, while the Urbach energy increased, reflecting enhanced structural disorder and the formation of localized electronic states. The refractive index and optical conductivity exhibited wavelength-dependent behavior and increased with GnP incorporation, consistent with enhanced electronic polarizability of the nanocomposites. Dispersion energy analysis based on the Wemple–DiDomenico model demonstrated that the dispersion energy (E_d)

exhibits a non-monotonic dependence on GnP content, highlighting the competing effects of interfacial disorder at low filler concentrations and improved electronic coupling at higher loadings. The evaluated nonlinear optical parameters, including third-order nonlinear susceptibility and nonlinear refractive index, increased with GnP concentration, indicating enhanced nonlinear optical response. Overall, the experimental results demonstrate that incorporating graphene nanoplatelets effectively tailors the electrical and optical properties of CS/PVP-based nanocomposites. These findings provide a systematic experimental framework for understanding the structure–property relationships in graphene-reinforced biopolymer systems and support their potential use in optoelectronic and energy-related applications.

Funding

No funds, grants, or other support was received.

Data availability statement

The data cannot be made publicly available upon publication because they are not available in a format that is sufficiently accessible or reusable by other researchers. The data that support the findings of this study are available upon reasonable request from the authors.

Author contributions

Ömer Bahadır Mergen 0000-0002-8829-436X
Conceptualization (lead), Formal analysis (lead), Investigation (lead), Methodology (equal), Resources (equal), Supervision (equal), Validation (equal), Visualization (lead), Writing – original draft (lead), Writing – review & editing (equal)

Ertan Arda 0000-0001-8679-0530
Methodology (equal), Resources (equal), Supervision (equal), Validation (equal), Writing – review & editing (equal)

References

[1] AlKhalifah M S, El Radaf I M and El-Bana M S 2020 New window layer of Cu2CdSn3S8 for thin film solar cells *J. Alloys Compd.* **813** 152169
[2] Al-Saleem N K, Al-Naghmaish A, Madani M, Alfawwar W, Elbasiony A M, Alharthi S, Haque M A and Ghobashy M M 2025 Multifunctional roles and advances of polymers in solar cell technologies: a review *RSC Adv.* **15** 35998
[3] Heiba Z K, Mouhammad S A, Badawi A and Mohamed M B 2025 Optoelectronic and energy storage characteristics of PVA/CMC/ZnCo2O4-CdS/MWCNTs/PANI nanocomposite *J. Macromol. Sci. Phys.* 1–23
[4] Mamand D M, Aziz D M, Khasraw S S, Al-Azzawi A G S, Al-Saeedi S I, Aziz S B and Hassan J 2025 Improved optical characteristics of PEO polymer integrated with graphene oxide *Sci. Rep.* **15** 32225
[5] Negut C C, Stefan-van Staden R and Ilie-Mihai R 2025 Progress and applications of nanocomposites in the technology of biosensors *Nanomater* **15** 1905
[6] Asih G I N, Rafryanto A F, Hartati S, Jiang X, Anggraini A, Yudhowijoyo A, Jiang J and Arramel 2025 Recent advances of polymer nanocomposites in emerging applications *CFM* **1** 20250105
[7] Aziz S B, Aziz D M, Muhammad D S, Hama P O and Abdullah O G 2025 Enhancing the optical properties of chitosan-based biopolymer for optoelectronic applications using natural dye extracted from hollyhock waste flowers *Opt. Mater.* **159** 116596
[8] Badawi A and Alharthi S S 2023 Enhancement the optical and electrical performance of PVA/MWCNTs blend via Cu/ZnS nanoparticles doping for flexible eco-friendly applications *Appl. Phys. A* **129** 372
[9] Abdelhamid H N 2023 Biodegradable polymers nanocomposites *SSRN* 1–36
[10] Mergen Ö B 2021 CS/PVA/PVP/GO Hibrit Kompozitlerin Hazırlanması ve Optik Bant Boşluğu Enerjilerinin Belirlenmesi *AKÜ FEMÜBİD* **21** 46–55
[11] Aziz S B 2017 Morphological and optical characteristics of chitosan(1−x):Cuox ($4 \leqslant x \leqslant 12$) based polymer nano-composites: optical dielectric loss as an alternative method for tauc's model *Nanomater* **7** 444
[12] Fen Y W, Yunus W M M, Yusof N A, Ishak N S, Omar N A S and Zainudin A A 2015 Preparation, characterization and optical properties of ionophore doped chitosan biopolymer thin film and its potential application for sensing metal ion *Optik* **126** 4688–92
[13] Mallakpour S and Khadem E 2018 Construction of crosslinked chitosan/nitrogen-doped graphene quantum dot nanocomposite for hydroxyapatite biomimetic mineralization *Int. J. Biol. Macromol.* **120** 1451–60
[14] El Sayed A M and Mohamad A D M 2018 Synthesis, structural, thermal, optical and dielectric properties of chitosan biopolymer; influence of PVP and α-Fe_2O_3 Nanorods *J. Polym. Res.* **25** 175
[15] Kausar A 2019 Polymer and modified chitosan-based nanocomposite: impending material for technical application *Polym.-Plast. Technol. Mater.* **58** 934–47
[16] Anas N A A, Fen Y W, Omar N A S, Ramdzan N S M, Daniyal W M E M M, Saleviter S and Zainudin A A 2019 Optical properties of chitosan/hydroxyl-functionalized graphene quantum dots thin film for potential optical detection of ferric (III) ion *Opt. Laser Technol.* **120** 105724

[17] Zainudin A A, Fen Y W, Yusof N A and Omar N A S 2017 Structural, optical and sensing properties of ionophore doped graphene based bionanocomposite thin film *Optik* **144** 308–15
[18] Mamand D M, Khasraw S S, Abdulwahid R T, Mohammed P A, Hassanzadeh A, Abdullah O G, Muhammad D S, Aziz S B and Hassan J 2025 Optical band gap reduction of polyethylene oxide through black iron (III) oxide nanoparticles insertion: Structural, magnetic, morphological and optical properties *J. Sci.: Adv. Mater. Devices.* **10** 100937
[19] Khasraw S S, Mamand D M, Saeed S R, Hama P O, Hassanzadeh A, Aziz D, Mohammed P A, Abdulwahid R T and Aziz S B 2025 PEO based nanocomposite with improved structural and optical properties *J. Inorg. Organomet. Polym. Mater.* **35** 6290–316
[20] Khasraw S S, Mamand D M, Saeed S R, Hassanzadeh A, Aziz S B and Abdullah O G 2025 Optoelectronic characteristics of PVA: Fe_3O_4 magnetic nanocomposite films *Int. J. Polym. Anal. Charact.* **30** 895–925
[21] Hamdi M, Nasri R, Li S and Nasri M 2019 Bioactive composite films with chitosan and carotenoproteins extract from blue crab shells: biological potential and structural, thermal, and mechanical characterization *Food Hydrocoll* **89** 802–12
[22] Usman F, Dennis J O, Seong K C, Ahmed A Y, Meriaudeau F, Ayodele O B, Tobi A R, Rabih A A S and Yar A 2019 Synthesis and characterisation of a ternary composite of polyaniline, reduced graphene-oxide and chitosan with reduced optical band gap and stable aqueous dispersibility *Results Phys.* **15** 102690
[23] Mergen Ö B, Arda E and Evingür G A 2020 Electrical, optical and mechanical properties of chitosan biocomposites *J. Compos. Mater.* **54** 1497–510
[24] Mergen Ö B and Arda E 2020 Determination of optical band gap energies of CS/MWCNT Bio-nanocomposites by Tauc and ASF methods *Synth. Met.* **269** 116539
[25] Khasraw S S, Mamand D M, Saeed S R, Hassanzadeh A, Abdullah O G and Aziz S B 2025 Structural, morphological, and optical properties of PVA polymer composites incorporated with various concentrations of GO: linear and nonlinear optoelectronic studies *J. Mater. Sci. Mater. Electron.* **36** 1067
[26] Sarhan A, Fahmy T and Habib A 2024 Optical, AC conductivity and antibacterial activity enhancement of chitosan-silver nanocomposites for optoelectronic and biomedical applications *Phys. Scr.* **99** 105905
[27] Garnica-Palafox I M, Velázquez-Benítez A M, Sánchez-Arévalo F M and Qureshi N 2025 Optical characterization of chitosan/poly (vinyl alcohol) hybrid hydrogels and the effect of genipin crosslinking and multiwalled carbon nanotube fillers *Opt. Mater.* **160** 116686
[28] Mamand D M *et al* 2025 Advanced spectroscopic approach for exploring the structural, optical, and electronic properties in dye-functionalized chitosan biopolymers *Spectrochim. Acta - A: Mol. Biomol. Spectrosc.* **329** 125485
[29] Kara S, Arda E, Dolastir F and Pekcan Ö 2010 Electrical and optical percolations of polystyrene latex–multiwalled carbon nanotube composites *J. Colloid Interface Sci.* **344** 395–401
[30] Mergen Ö B 2021 Effect of MWCNTaddition on the optical band gap of PVA/CS transient biocomposites *J. Compos. Mater.* **55** 4347–59
[31] Mergen Ö B and Arda E 2023 Determination of electrical and optical behaviors of carboxymethyl cellulose/graphene nanocomposites *J. Mater. Sci. Mater. Electron.* **34** 1719
[32] Heiba Z K, El-naggar A M, Kamal A M, Aldhafiri A M and Mohamed M B 2023 Influence of polyaniline on the structural, linear/nonlinear optical, and dielectric characteristics of poly(vinyl chloride/poly (ethylene oxide) blends *J. Polym. Sci. Part B* **63** 343–60
[33] Aziz D M, Mohammed S J, Mohammed P A, Al-Zangana S, Aziz S B, Muhammad D S, Abdulwahid R T, Darwesh A H A and Hussein S A 2025 Spectroscopic study of wemple-didomenico empirical formula and taucs model to determine the optical band gap of dye-doped polymer based on chitosan: common poppy dye as a novel approach to reduce the optical band gap of biopolymer *Spectrochim. Acta - A: Mol. Biomol. Spectrosc.* **325** 125142
[34] Mergen Ö B and Arda E 2023 Electrical, optical and dielectric properties of polyvinylpyrrolidone/graphene nanoplatelet nanocomposites *Opt. Mater.* **139** 113823
[35] Mohammed M I and Yahia I S 2022 Towards multifunctional applications of Fullerene-filled (PVA-PEG) polymeric nanocomposite films: structural, optical, and electrical properties *Phys. Scr.* **97** 065813
[36] El-naggar A M, Heiba Z K, Kamal A M, Abd-Elkader O H, Abdellatief M and Mohamed M B 2023 PVC polymer/ZnO/NiO/Co3O4 nanocomposites: toward improved optical properties *J. Vinyl Addit. Technol.* **30** 44–58
[37] El Radaf I M 2019 Structural, optical, optoelectrical and photovoltaic properties of the thermally evaporated Sb2Se3 thin films *Appl. Phys. A* **125** 832
[38] Mohamed F, Sharmoukh W, Youssef A M and Hameed T A 2022 Structural, morphological, optical, and dielectric properties of PVA-PVP filled with zinc oxide aluminum-graphene oxide composite for promising applications *Polym. Adv. Technol.* **33** 1009–20
[39] Heiba Z K, Kamal A M, El-naggar A M, Mohamed M B, Abdel-Kader M H and Alharby T 2023 Reinforcement of linear/nonlinear optical and dielectric characteristics of PVC/PEG blend based on CeO_2/TBAI filler *Inorg. Chem. Commun.* **158** 111624
[40] El-naggar A M, Heiba Z K, Kamal A M, Altowairqi Y, Mohamed M B, Abd-Elkader O H and Alhazime A A 2022 Influence of nanocomposite (1-x)CdS/xCuS on optical characteristics of PVA/CMC/PEG blended polymer; effect of ratio (x) *Opt. Mater.* **133** 112923
[41] Veena G and Lobo B 2019 Dispersive parameters of oxidized PVA-PVP blend films *Turk. J. Phys.* **43** 337–54
[42] Atta A, Abdeltwab E, Negm H, Rabia M and Abdelhamied M M 2023 Fabrication of polypyrrole/graphene oxide polymer nanocomposites and evaluation of their optical behavior for optoelectronic applications *J. Inorg. Organomet. Polym.* **33** 4083–95
[43] El Radaf I M, Al-Zahrani H Y S and Hassanien A S 2020 Novel synthesis, structural, linear and nonlinear optical properties of p-type kesterite nanosized Cu_2MnGeS_4 thin films *J. Mater. Sci. Mater. Electron.* **31** 8336–48
[44] Ahmed K K, Aziz S B, Abdulwahid R T, Hussen S A and Brza M A 2022 Green synthesized Al-metal complex to reduce the crystalline phase and improve the optical properties of CS based polymer blends *Opt. Mater.* **134** 113112
[45] Darwesh A H, Mohammed P A, Mamand S M, Hussen S A, Aziz S B, Brza M A, Abdullah R M and Karim W O 2023 Investigation of structural and optical characteristics of biopolymer composites based on polyvinyl alcohol inserted with PbS nanoparticles *Coatings* **13** 578
[46] Muhammad D S, Aziz D M and Aziz S B 2025 The impact of green chemistry to synthesize PVA/cobalt metal complexes (CoMCs) composites with enhanced optical behavior *Opt. Mater.* **158** 116448
[47] Mohamed M B, El-naggar A M, Heiba Z K and Kamal A M 2024 Modifications in the structural, optical, and dielectric properties of PVA/PVP/PEG blend by incorporation of PANi/ZnWO4 nanohybrid for optoelectronic and energy storage devices *Opt. Mater.* **149** 115047
[48] Hassanien A S and El Radaf I M 2020 Optical characterizations of quaternary Cu_2MnSnS_4 thin films: novel synthesis process of film samples by spray pyrolysis technique *Physica B Condens. Matter.* **585** 412110

[49] Badawi A and Alharthi S S 2023 Enhancement the optical and electrical performance of PVA/MWCNTs blend via Cu/ZnS nanoparticles doping for flexible eco-friendly applications *Appl. Phys. A* **129** 372
[50] El Radaf I M 2020 Structural, optoelectrical, linear, and nonlinear optical characterizations of the $Cu_2ZnGeSe_4$ thin films *J Mater Sci: Mater Electron* **31** 3228–37
[51] Farag A A M, Yahia I S, Yakuphanoglu F, Kandaz M and Farooq W A 2012 Optical properties and the dispersion parameters of new zinc Phthalocyanine benzofuran derivative prepared by non-vacuum spin coating technique *Opt. Commun.* **285** 3122–7
[52] Saini I, Sharma A, Dhiman R, Aggarwal S, Ram S and Sharma P K 2017 Grafted SiC nanocrystals: for enhanced optical, electrical and mechanical properties of polyvinyl alcohol *J. Alloys Compd.* **714** 172–80
[53] Ghazy A R, Al-Hossainy A F, El-Sheekh M M and Makhlof M E M 2023 Investigating the differences in structure, morphology, optical properties, laser photoluminescence and dielectric properties for chitosan-doped commercial and Polycladia myrica mediated ZnO nanoparticles films combined with TD-DFT simulations *Algal Res.* **71** 103076
[54] Hameed T A, Mohamed F, Turky G and Salama A 2022 Carboxymethylcellulose/polyvinylpyrrolidone filled with Al-doped ZnO nanoparticles as a promising film for optoelectronic applications *Opt. Mater.* **134** 113097